J. Fluid Mech. (1992), *vol.* 241, *pp.* 525–548
Printed in Great Britain

Unsteady shock propagation in a steady flow nozzle expansion

By R. J. STALKER[1] AND N. R. MUDFORD[2]†

[1] Department of Mechanical Engineering, University of Queensland, Brisbane, Qld 4072, Australia

[2] Department of Physics and Theoretical Physics, Australian National University, Canberra, ACT 2601, Australia

(Received 2 February 1989 and in revised form 22 January 1992)

The flow field produced when a strong shock wave propagates into a steady flow expansion has been investigated numerically, experimentally and analytically. The experiments were conducted with a shock tube which was modified to allow steady flow to be established in a hypersonic nozzle prior to arrival of the shock. It has been found that the axial density distribution associated with the prior steady flow allows the unsteady flow following the nozzle primary starting shock to accelerate from supersonic to hypersonic speeds, whereas a uniform density distribution causes it to decelerate to subsonic speeds. The prior steady flow also allows the starting shock system to propagate through the nozzle at nearly the same velocity as the incident primary shock, and therefore provides a convenient method of ensuring rapid steady flow initiation in shock tunnel nozzles. The analysis shows that the flow behaviour can be understood in terms of two approximate models. The first is applicable to a wide range of flow conditions, and allows calculation of the trajectory of the centre of mass of the starting shock system. The second is applicable to cases involving a prior steady flow, and predicts detailed features of the flow structure.

1. Introduction

When a shock wave propagates along a constant area tube, into a gas of constant density, its behaviour is determined by the pressure and velocity at the interface between the shock compressed gas and the agency driving it. If this pressure and velocity remain constant, then so does the shock velocity. This is because the momentum required to accelerate the gas which is continually swept up by the shock front ultimately is provided by the impulse of the pressure at the interface.

However, if the shock encounters an expanding area change within which the density is the same as that in the shock tube, then the momentum change required to bring the extra gas within the increased area up to the speed associated with the shock is more than can be provided by the pressure impulse of the gas layers following the shock, and it must slow down. The resulting unsteady flow is a member of a class of such flows with initial uniform density, and these have been studied by a number of investigators (e.g. Ackroyd 1964; Smith 1966). They have shown that the use of initial densities as high as those in the shock tube can severely limit the utility of steady expansion nozzles in shock tube flows, by extending the period over which transient phenomena dominate.

† Present address: Department of Mechanical Engineering, University College, University of New South Wales, Australian Defence Force Academy, Northcott Drive, Campbell, ACT 2601, Australia.

If, on the other hand, the shock encounters an area change within which the gas density varies in a suitable manner then, in principle, it may be possible to arrange that the momentum change needed to bring the gas initially resident in the nozzle up to the required speed may be provided by the gas layers following the shock. The shock therefore maintains its speed, and the duration of the transient effects associated with the passage through the nozzle is reduced.

For strong shock waves, the required density distribution in the resident gas can be approximated by providing a steady flow through the nozzle prior to arrival of the shock wave, and this situation is studied in this paper. As indicated in a previous paper (Mudford & Stalker 1976) the reduction in the duration of the transient effects is sufficient to allow this prior steady flow method to be as effective as more conventional methods in ensuring rapid establishment of steady flow in an expansion nozzle in a shock tube, but with an important advantage. Conventional methods minimize the impedance of the gas initially resident in the nozzle by pre-evacuating the nozzle volume, providing a diaphragm between the shock tube and the nozzle in order to ensure that the initial shock tube density remains at the correct value. The diaphragm is ruptured on arrival of the shock but unfortunately, the fragments cannot be swept away in the short test times, of the order of 20–30 μs, which are a feature of high-velocity shock tubes. By eliminating the diaphragm, the prior steady flow makes it possible to generate a high enthalpy hypersonic flow with a high velocity shock tube.

Thus, the prime purpose of the study reported here was to develop an understanding of a technique for producing high enthalpy hypersonic non-reflected shock tunnel flows. As observed above, the test times obtained in such shock tunnels generally are more than an order of magnitude less than in reflected shock tunnels, but they have the compensating advantages that they are able to operate at higher stagnation enthalpies and at higher effective nozzle reservoir pressures. The short test times obviously restrict the types of flow which can be studied, but it is worth recording that steady flow over blunt and slender bodies has been demonstrated in such a shock tunnel (Oertel 1970), while the shock tunnel used in the present experiments also has been employed for experiments on high enthalpy nozzle flows (Mudford & Stalker 1980), ionizing hydrogen flow over a wedge (Stalker 1980) and dissociation effects on the flow downstream of a blunt nose (Macrossan 1990).

The interaction of a shock with an expanding flow may occur in other situations, such as in a pulsed exhaust, or behind the primary shock in an explosion, where the shock induced motion leads to an expanding flow of the gas, which may be followed by a second shock. The ideas developed here may assist in understanding such flows.

The paper begins with a general description of the flow, as observed in experiments with air test gas. Numerical calculations, employing the method of characteristics, then are used to demonstrate the differences in flow behaviour with and without the prior steady flow. These calculations were performed for helium test gas, and are checked against experiments. Streak interferograms obtained in experiments with air are also presented, and show the same differences in flow behaviour.

Two simplified, approximate, flow models are then developed. These models not only serve a predictive purpose but, by restricting attention to dominant phenomena, they make it easier to understand the overall flow behaviour. One model predicts the trajectory of the starting shock system, and applies to a wide range of initial nozzle conditions. The other applies when a prior steady flow is present, and is concerned with details of the flow structure.

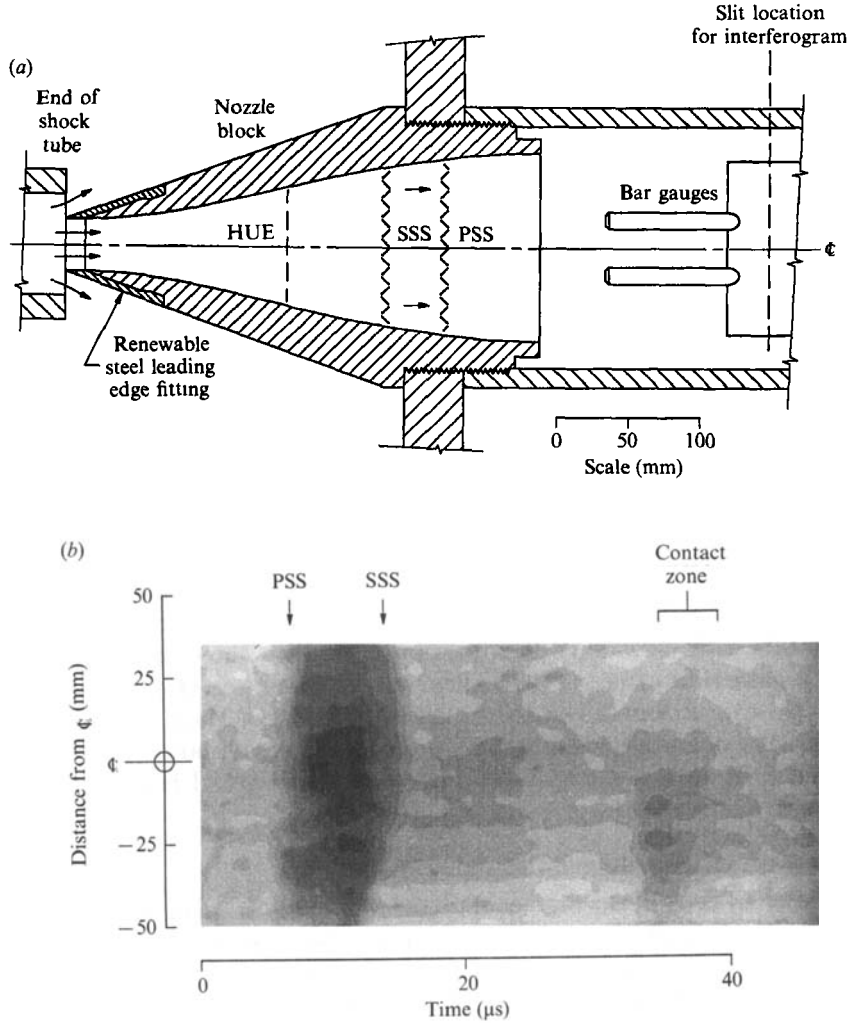

FIGURE 1. (*a*) Expansion nozzle. PSS, primary starting shock; SSS, secondary starting shock; HUE, head of unsteady expansion. Nozzle dimensions: inlet diam. 38 mm, exit diam. 132 mm, length 300 mm. (*b*) Time resolved vertical slit interferogram taken with prior flow and air test gas. Shock-tube fill pressure = 1.7 kPa; shock speed = 7.6 km s^{-1}.

2. Description of flow field

The axisymmetric steady flow expansion nozzle, as used in the experiments reported below, is shown in figure 1. The incident primary shock (IPS) enters from the upstream direction, to the left of the figure. The central core of the test gas following the IPS enters the hypersonic nozzle and initiates the unsteady flow which precedes the steady test flow. The remainder of the post-IPS gas is deflected into the reservoir which surrounds the shock tube and nozzle, and ceases to be of interest. The post-IPS gas conditions are thus the nozzle entrance conditions and, clearly, must be supersonic in order that the test-section flow be hypersonic. This implies that the IPS must be sufficiently strong for this condition to be satisfied.

A typical unsteady flow pattern observed in the nozzle is shown at the bottom of

figure 1. This is a time-resolved Mach–Zehnder interferogram, which has been obtained by viewing the test section through a vertical slit which was, as shown in the figure, normal to the flow direction. The bar gauge assembly shown in the figure was absent for the interferogram. The fringe shifts on the original interferogram were measured by a scanner linked to a computer, and are displayed as grey scale coded contours of fringe shift which may, for the present purpose, be interpreted as contours of density integrated over the path length through the test-section flow. The contours show that the density gradients are predominantly in a direction parallel to the flow direction and therefore that, for the purposes of analysis, it is a reasonable approximation to assume one-dimensional flow, in which flow properties are constant in planes normal to the nozzle axis.

The flow structure which is revealed by the interferogram is qualitatively similar to those recorded by Smith (1966) for flows with initially uniform resident gas density, and is represented schematically in the top figure as it would appear at an instant in time. In passing into the nozzle, the IPS becomes the primary starting shock (PSS) which is witnessed in the interferogram as the earliest rise in density. This is followed soon after on the interferogram by a fall in density, which is identified as the secondary starting shock (SSS), as shown on the figure. It will be seen below that, although this shock faces upstream, it is swept downstream by the flow. It will also be seen that the head of an unsteady expansion wave (HUE) may occur further upstream, but the sensitivity of the interferogram is not adequate to detect this with certainty. The interferogram also shows a weak zone of increased density some time after the SSS. This is thought to be a very weak compression wave, arising from a mismatch in driver gas and test gas Mach numbers at the contact surface. Although this mismatch is thought to have a marginal effect on some of the experimental data reported below, it is not investigated here.

3. Method of characteristics calculations

In order to explain the observed features of the flow, to identify other features, and to explore the mechanisms by which they arise, a series of perfect gas calculations was performed using the unsteady one-dimensional method of characteristics (Mudford 1976). Following Rudinger (1955) the calculations were conducted with the speed of sound, the specific entropy, and the flow speed as dependent variables. The flow along stream trajectories was isentropic, except when they crossed shock waves, and there the conditions at the post shock points were calculated by intersecting the shock trajectory with the characteristic, left or right running as appropriate, which intersected it from behind. Compatibility then was achieved through simultaneous solution of the shock jump relations and the compatibility relation applying along the intersecting characteristic.

While the interferogram of figure 1 indicates that the flow is essentially one dimensional, the fact that the nozzle is contoured implies that, at least in steady flow, the streamwise rate of expansion of the test gas will tend to vary across the nozzle, with the most rapid expansion on the centreline. In order to allow for this effect in the calculations, a nozzle area ratio distribution was selected which produced a rate of expansion close to that of an average streamtube. A comparison of the assumed and actual area ratio distributions is shown at the bottom of figure 2.

Calculations were performed for helium test gas, yielding the results shown in figures 2 and 3. Paying attention first to the wave diagrams in figure 2, the flow structure both with and without the prior steady flow displays the PSS and SSS

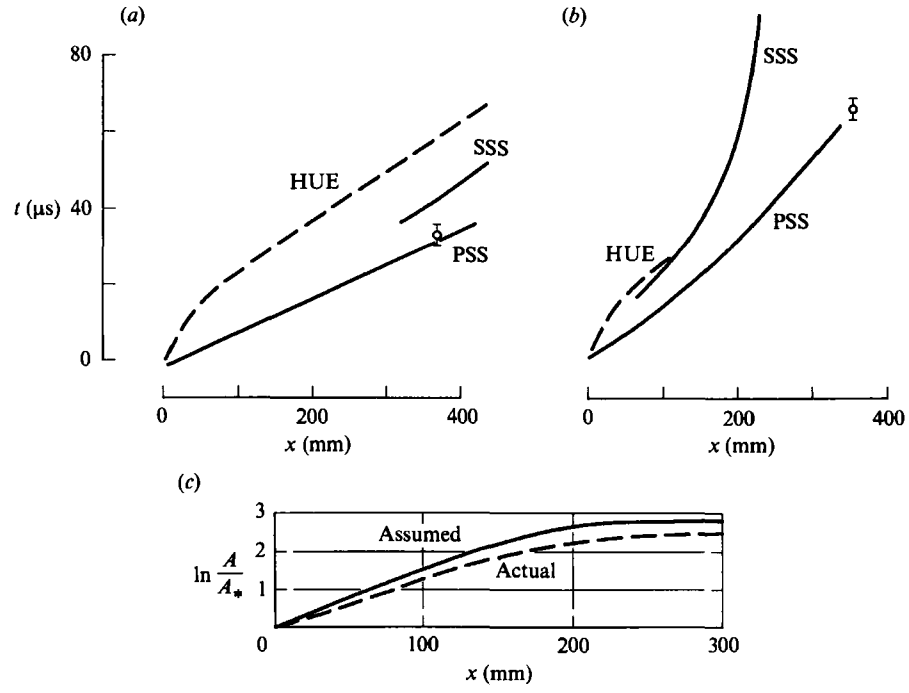

FIGURE 2. (*a*) Wave diagram with PSF. (*b*) Wave diagram without PSF. Helium test gas. Shock-tube fill pressure = 6.8 kPa; shock speed = 9.0 km s^{-1}; t = time from incident primary shock arrival at nozzle entrance; x = downstream distance from nozzle entrance. ○, experiments – time of arrival of primary starting shock. (*c*) Nozzle profiles. A = nozzle area; A_* = value at inlet.

observed in figure 1. The IPS propagates into the nozzle as the PSS, and forms the downstream boundary to the unsteady flow. With a prior steady flow, as in figure 2(*a*), the upstream boundary is formed by the leading edge of an expansive disturbance, which propagates as the HUE. As discussed below, this disturbance arises from the mismatch, at the nozzle entrance, between the prior steady flow and the post-IPS flow. Because it propagates into the steady test flow at the local speed of sound, the trajectory of the HUE is a left-running characteristic of the steady flow expansion, through the nozzle, of the post-IPS gas. However, because there is no means of providing significant acceleration of the PSS as it passes down the nozzle, gas which has been accelerated by the nozzle tends to overtake gas which has been processed by the PSS and to prevent this, a compression wave forms which tends to coalesce into the SSS. This upstream-facing shock tends to be swept downstream as part of the starting shock system. In the absence of a prior steady flow, as shown in figure 2(*b*), the PSS slows down as it passes through the nozzle, causing the SSS to become so strong that it does not pass downstream as rapidly as the HUE. It therefore passes through the HUE, to become the upstream boundary of the unsteady flow, in place of the HUE.

It will be noted that, in figure 2(*b*), the SSS becomes nearly stationary. This arises because of the choice of area ratio. As shown in figure 4, if it is imagined that the nozzle is continued far downstream at the maximum area, and the post-IPS flow into the nozzle is maintained indefinitely, then a 'quasi-steady' flow is established, in which the nozzle flow is steady, and the speed and pressure change across the PSS, and hence the SSS, are matched to the nozzle exit conditions. These conditions therefore

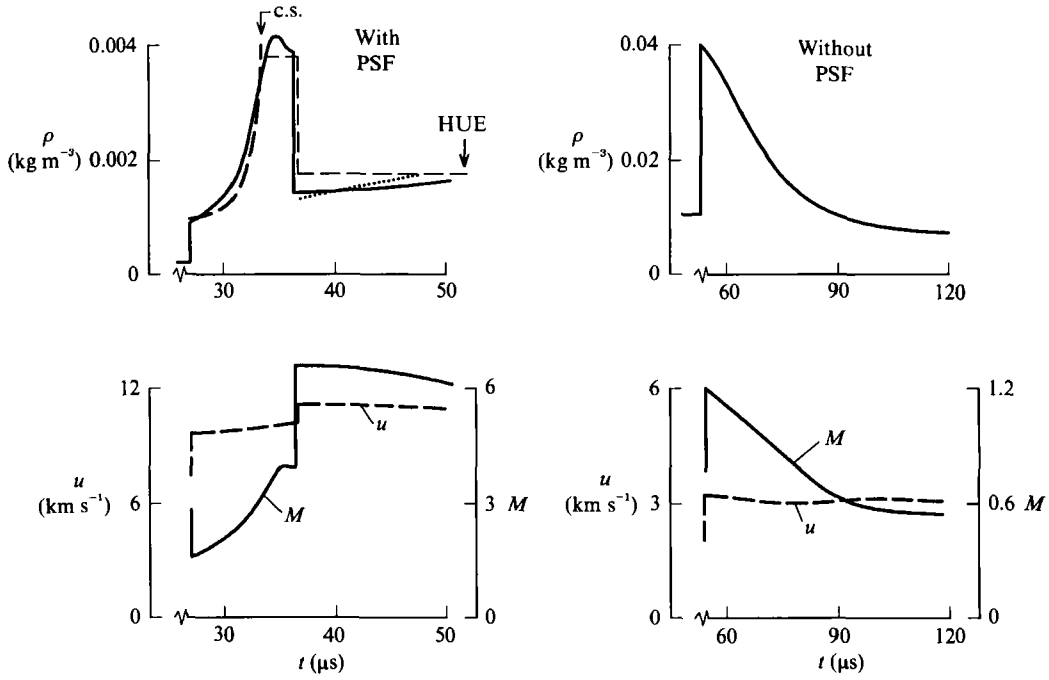

FIGURE 3. History of nozzle exit conditions. Helium test gas. Shock-tube fill pressure = 6.8 kPa; shock speed = 9.0 km s^{-1}; t = time from incident primary shock arrival at nozzle entrance; u = flow velocity; M = Mach number; ρ = density; cs = contact surface; ———, approximate theory; ....., unsteady expansion according to approximate theory.

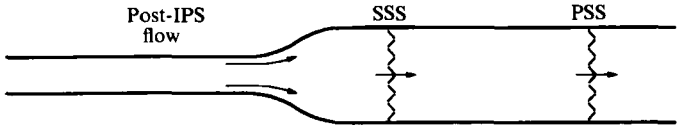

FIGURE 4. Asymptotic quasi-steady, flow.

govern the speed at which the SSS moves downstream. Calculations for the flow of figure 2(*b*) indicate that the quasi-steady speed of the SSS is very small, and that it is approaching this condition in the figure. If the area ratio were significantly larger, then the SSS would remain within the nozzle, and a useful steady test flow never would be established. If it were smaller, then the SSS would be swept out of the nozzle more rapidly.

The expected effect of the prior steady flow on the PSS trajectory, as outlined in the introduction, is clearly observed in the figure. With a prior steady flow, the PSS speed is nearly constant but, with no prior flow, the PSS speed falls by more than a factor of two in passing through the nozzle.

Consequences of this difference are shown in figure 3, where the temporal variation of flow quantities at a station near the nozzle exit are displayed. Noting the Mach number first, it can be seen that in both cases, the immediate post-PSS value is close to 1.3, which is appropriate to a strong shock. (In the case of the prior steady flow, the initial resident gas velocity leads to a post-PSS Mach number slightly in excess of 1.3.) However, the Mach number then falls rapidly to subsonic values for no prior flow, whilst for the prior steady flow case, it rises to hypersonic values.

This change is due to a reversal in the relative dominance of two effects, both of which are associated with the fact that the gas which passes the nozzle exit subsequent to the PSS has come from further upstream in the nozzle. One effect is that expansion of this gas in passing down the nozzle will tend to cool it, causing the temperature at the nozzle exit to decay. The other effect is that, if the gas was processed by a stronger PSS before it began its passage towards the nozzle exit, then the entropy rise associated with that shock will tend to cause the temperature at the nozzle exit to rise. Noting from figure 3 that, except for a modest jump in velocity at the SSS for the prior steady flow case, the velocity remains nearly constant, these respective tendencies will be evidenced by rising and falling Mach numbers. Thus, in the prior steady flow case, where the PSS speed is constant, the cooling effect dominates, and in the no prior flow case, the effect of the axial entropy gradient induced by the attenuation of the PSS dominates.

Figure 3 also shows the density history at the nozzle exit. It can be seen that for no prior flow, the maximum density occurs at the PSS, whereas with prior steady flow, it occurs close to the SSS. The maximum density level obtained with the prior steady flow is a factor of 10 less than that obtained with no prior flow, but Pitot pressure levels differ by less than a factor of two. This is because of the higher velocities associated with prior steady flow. Given that Pitot pressures are of the same order, the higher Mach numbers of the prior steady flow case imply that it must also exhibit lower static pressures.

Finally, the HUE is indicated in figure 3 for the prior steady flow case and it can be seen that, although the non-steady expansion fan persists for a substantial period, it is very weak indeed. In fact, for many practical purposes, this could be regarded as part of the steady flow. This is an important feature in the hypersonic shock-tunnel context, since it can be expected to contribute to the useful test flow period – either as a direct extension of that period, or by providing a 'nearly steady' period, during which transient effects in the model flow can decay, before the true steady flow arrives.

4. Experiments

Experiments were conducted with the nozzle shown in figure 1, using the free-piston shock tunnel T3 at the Australian National University. The shock tunnel is described elsewhere (Stalker 1972), and only the modifications made to permit non-reflected operation with a prior steady flow are described here.

As shown in figure 5, the shock tunnel involves a compression tube 6 m long and 300 mm in diameter, driving a shock tube 8 m long and 76 mm in diameter. For these experiments the downstream 2 m of the shock tube was surrounded by a nozzle feed tank. The test section was vented to the dump tank via a valve assembly, which was spring loaded to open. The valve actuating sleeve was rigidly connected to the shock tube, and held the valve closed before a test. It was pierced in order to allow a clear view of the test section flow by use of the test section windows. When the shock tunnel was fired, the motion of the relatively heavy free piston along the compression tube caused the compression tube–shock tube assembly to recoil, and the valve actuating sleeve to retract. The valve therefore opened, to allow the pre-evacuated dump tank to exhaust gas from the test section, and thereby set up the prior steady flow. A no prior flow test was accomplished by allowing the valve to remain open before a test, with the dump tank and test section filled to the initial shock tube pressure. The valve opening time was about 50 ms, which was necessary to ensure

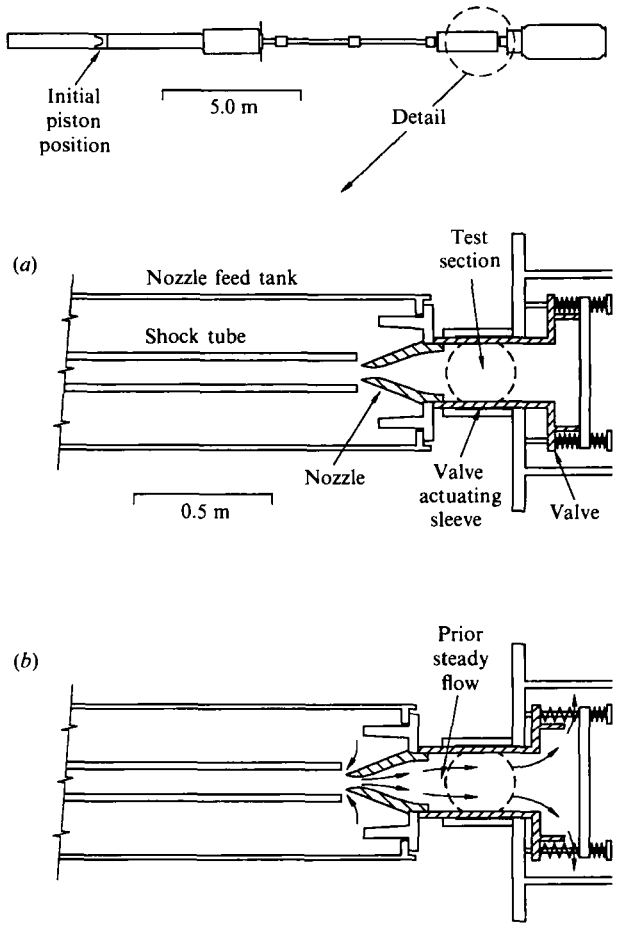

FIGURE 5. Experimental shock tunnel configuration. (*a*) Before test. (*b*) After recoil.

that the prior steady flow was established before the primary shock wave arrived at the nozzle. The volume of the nozzle feed tank was large enough to ensure that the pumping action of the prior steady flow altered the shock tube pressure by no more than an estimated 4% during this period, when air or argon was used as test gas. With helium, a 10% change may have been possible. The entrance to the nozzle was 38 mm in diameter. The nozzle was contoured (Mudford & Stalker 1980) to produce parallel flow at the test section with an area ratio of 16 but, in order to minimize test time losses, it was truncated at 300 mm from the nozzle entrance, yielding an exit diameter of 132 mm.

Two methods were used to observe the unsteady flows. For tests with helium, bar gauges were mounted to measure test section Pitot pressure, as shown in figure 1. The upstream ends of these gauges were 350 mm from the nozzle entrance and each was 19 mm off the nozzle centreline. With air, where gas refractivities were higher, it was possible to make use of time resolved interferograms, obtained with a Carl Zeiss Mach Zehnder interferometer. The associated optical system was masked so that, in effect, the test section was viewed through a slit, approximately 130 mm long and 2 mm wide. An exploding wire was used as a light source, and the interferograms were recorded with an STL model 1D image converter camera. The experiments were

performed with helium driver gas, with a main diaphragm bursting pressure of 30 MPa, and an initial compression tube filling pressure of 32 kPa.

In order to check that the prior steady flow was established in the nozzle before the IPS arrived, PSS fringe shifts at the nozzle exit were measured. These were found to compare satisfactorily with fringe shifts calculated using the post-PSS gas properties, as obtained from the shock speed measurements and the predicted prior steady flow densities. Since the shock density ratio at a given shock speed is only weakly dependent on the pre-shock density, it follows that the shock fringe shifts could serve as a measure of the pre-shock density. They therefore confirmed that the prior steady flow density distribution had been established in the nozzle.

5. Comparison with experiment – general flow features

Figure 6 shows bar gauge Pitot pressure measurements. Helium test gas was used because stress wave reflection at the mounted end of the bar gauge limited the useful measurement period of the bar gauges to 80 μs, and helium allowed perfect gas pressure histories to be obtained within this relatively short period for all of the unsteady part of the flow. The measurements are compared with predictions derived from the method of characteristics computations of figures 2 and 3. For flow Mach numbers above one, Pitot pressures were calculated from the computational results by using the Rayleigh Pitot formula (Liepmann & Roshko 1957) modified to reference the Pitot pressure to the product of density and (velocity)^2. When the flow Mach number was less than one, the Pitot pressure was equated to the local flow reservoir pressure.

The bar gauge was 12 mm in diameter, with a blunt nose. When subjected to an increase in Pitot pressure, such as accompanies the passage of a shock wave, such a configuration experiences a pressure overshoot, followed by relaxation back to the new Pitot pressure level (Davies 1964). For the conditions of these tests, the characteristic time of such relaxation was typically 2 μs. This effect, together with a tendency for the gauges to exhibit small amplitude 'ringing' at a frequency of 500 kHz, meant that the gauges were only able to follow the Pitot pressure variation approximately, but this is sufficient for the purposes of comparison. It can be seen that, to within the accuracy allowed by the bar gauge dynamics, agreement with the computations is obtained both for prior steady flow and no prior steady flow. The fall in bar gauge pressure at $t = 14$ μs in the no prior flow case is thought to be due to the arrival at the bar gauge of the expansion wave originating from the rim of the nozzle exit. This occurs in this case because of the subsonic character of the flow at the nozzle exit.

The time of arrival of the PSS, as detected by the bar gauges, also is displayed in figure 2. The difference in PSS attenuation between prior steady flow and no prior flow is evidenced by this measurement which, in both cases, is consistent with the predictions. When combined with the successful prediction of approximate magnitude and time dependence of Pitot pressure, which has already been noted, it affirms the validity of the flow model represented by the method of characteristics calculations.

The interferograms provided an opportunity to examine flows with strong real gas effects. By aligning the viewing slit parallel to the axis of the nozzle, and sweeping the image of the slit across the imaging plane of the optical system, time resolved interferograms such as those displayed in figure 7 were obtained. For an undisturbed flow field, the fringes would remain vertical but, as the unsteady flow sweeps through

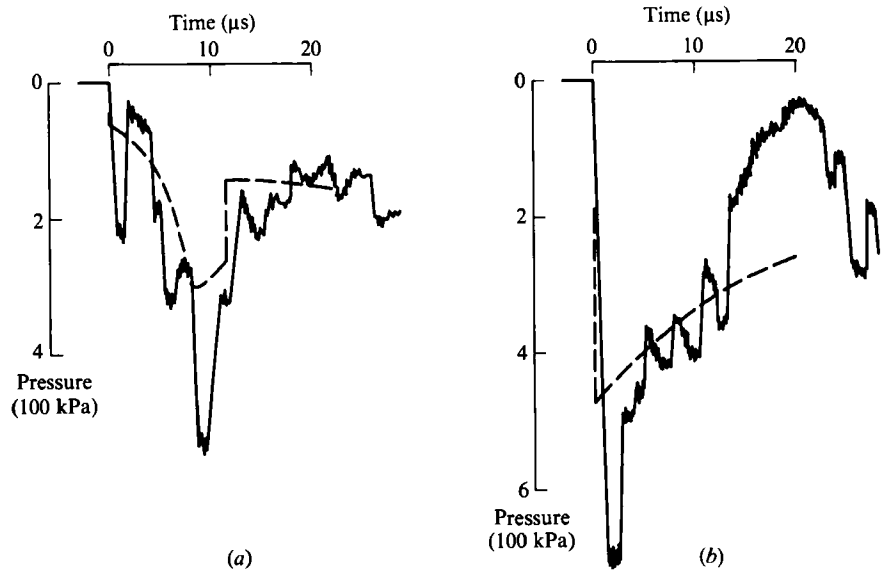

FIGURE 6. Time resolved Pitot pressure – effect of prior steady flow. Helium test gas. Shock-tube fill pressure = 6.8 kPa. Incident primary shock speed is (*a*) 9.2 km s^{-1} with prior steady flow; (*b*) 8.7 km s^{-1} without prior steady flow. ——, Bar gauge pressure records; ------, method of characteristics calculation of Pitot pressure.

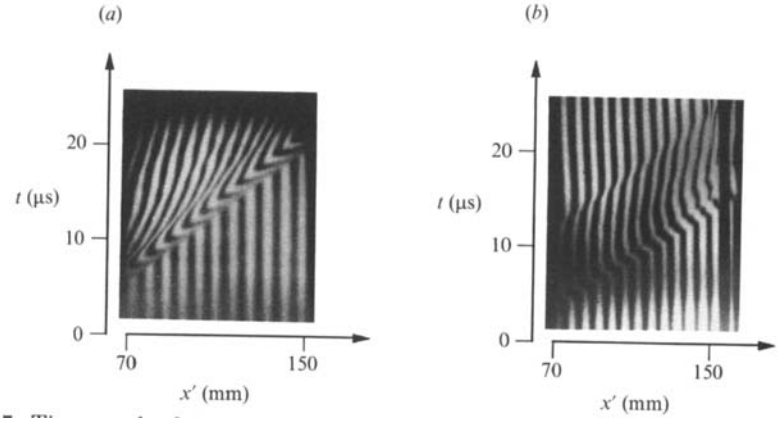

FIGURE 7. Time resolved interferograms – effect of prior steady flow. Air test gas. Shock-tube fill pressure = 0.8 kPa, incident primary shock speed = 8.2 km s^{-1}, (*a*) without prior steady flow, (*b*) with prior steady flow. x' = distance from nozzle exit. Wavelength of light used = 533 ± 5 nm.

the test section, the density changes cause the fringes to shift laterally. It can be seen that the fringe shifts with prior steady flow, as in figure 7 (*b*), are much smaller than with no prior flow, as in figure 7 (*a*). Real gas effects were revealed by fringe shift measurements in interferograms such as figure 7 (*b*), and are discussed below.

6. Approximate analytical model – shock system centre of mass

There are occasions, not all of which are restricted to the prior steady flows which are the main theme of this study, when knowledge of the behaviour of an unsteady shock system such as the present one is required. For example, when different nozzles

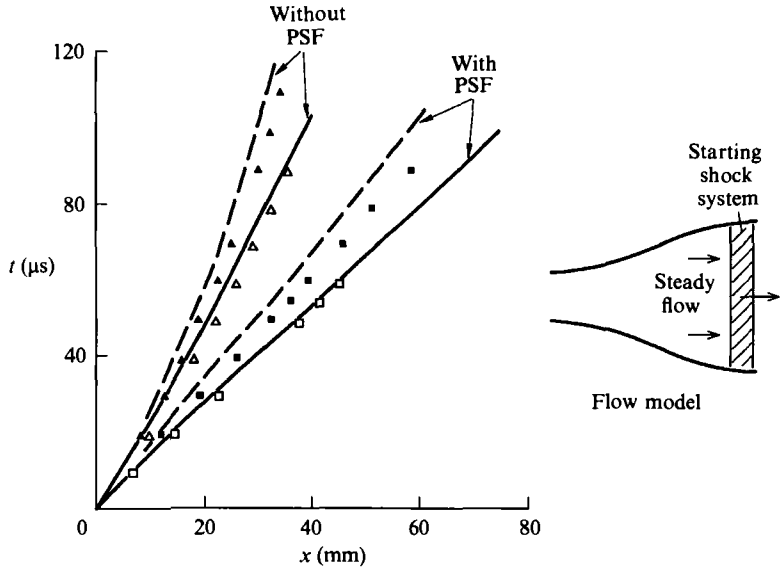

FIGURE 8. Starting shock system centre of mass trajectories. t = time from incident primary shock arrival at nozzle entrance; x = downstream distance from nozzle entrance. Perfect gas $\gamma = 1.4$, incident primary shock speed = 7.1 km s^{-1}. Method of characteristics: □, prior steady flow; △, no prior steady flow; ——, approximate analysis. Perfect gas $\gamma = 1.67$, incident primary shock speed = 6.6 km s^{-1}. Method of characteristics: ■, prior steady flow; △, no prior steady flow; – – –, approximate analysis.

are used, perhaps with different area ratios, or constraints such as the use of a large model in a shock tunnel are expected to lead to imperfect establishment of the prior steady flow, or the effect of a varying resident gas density which is not that of a prior steady flow is desired. The method of characteristics calculation is clearly too tedious to be employed conveniently for each such case, especially when real gas effects are involved. Therefore a relatively simple calculation method is required – particularly one which will yield the speed with which the unsteady shock system will pass through the nozzle.

By making a number of simplifying assumptions it is possible to write a momentum balance equation for the gas entrained between the PSS and the SSS. Solution of this single equation then provides an approximation to the trajectory of the centre of mass of the starting shock system. The assumptions made are:

(i) The flow is one-dimensional;
(ii) Nozzle area changes, and consequently flow property changes, are small over the width of the shock system;
(iii) The gas ahead of the shock has negligible momentum;
(iv) The gas flow conditions upstream of the shock system are taken to be those of the steady flow.

These assumptions lead to the model shown on the right of figure 8.

Assumption (iv) implies that, in cases where an unsteady expansion exists upstream of the shock system, the change in momentum across it is ignored. One effect of this assumption is to limit the shock system speed to that of the steady test flow. This restriction was often significant close to the beginning of the trajectory for the prior steady flow case, where the shock system mass was low and the pressure

impulse predicted a larger shock system speed. However, it was not important in later sections of the trajectory, or in any region of the no prior flow calculations, and therefore it is not expected to lead to significant errors for the types of flow studied here. However, for other flows, such as those involved with a reflected shock tunnel, it may be necessary to take account of the unsteady expansion.

The integrated momentum equation for the shock system centre of mass can now be written as

$$\int_0^t u\,\mathrm{d}m + \int_0^t (p-p_\mathrm{r})A\,\mathrm{d}t - \left\{m + \int_0^x \rho_\mathrm{r} A\,\mathrm{d}X\right\}(\mathrm{d}X/\mathrm{d}t) = 0, \tag{1}$$

with

$$m = \int_0^t \mathrm{d}m = \int_0^t \rho A(u-\mathrm{d}X/\mathrm{d}t)\,\mathrm{d}t, \tag{2}$$

where (X,t) are the coordinates of the shock system centre of mass in (x,t) coordinates, p, ρ and u are the pressure, density and velocity upstream of the shock system, m is the mass which has passed through the SSS in time t, A is the cross-sectional area at X, and p_r and ρ_r are the resident gas density and pressure ahead of the PSS. The first term in (1) represents momentum addition due to entry of the gas through the SSS. The second term represents the impulse from the pressure differential across the system and the third term is the resultant system momentum. Remembering that ρuA is constant, (1) and (2) can be rearranged to yield

$$\left\{\rho uAt - \int_0^x \rho A\,\mathrm{d}X + \int_0^x \rho_\mathrm{r} A\,\mathrm{d}X\right\}(\mathrm{d}X/\mathrm{d}t) = \rho uA\int_0^t u\,\mathrm{d}t - \rho uAX + \int_0^t (p-p_\mathrm{r})A\,\mathrm{d}t. \tag{3}$$

Some additional approximations allow further simplification (Stalker & Mudford 1973). Assuming that $p_\mathrm{r} \ll p$, and noting that $p/(\rho u^2) \sim M^{-2}$, where M is the Mach number, the last term on the right-hand side of (3) may be neglected for a nozzle which is predominantly hypersonic. In such a nozzle flow, u and ρA also may be taken to be constant along the nozzle and (3) becomes, after some manipulation and integration with respect to t,

$$(ut-X)^2 = 2\int_0^X (\rho A)^{-1}\left(\int_0^X \rho_\mathrm{r} A\,\mathrm{d}X\right)\mathrm{d}X. \tag{4}$$

Equation (4) demonstrates the importance of the resident gas density in the nozzle. When this density is sufficiently small compared to the test gas density, then the right-hand side of (4) is small, and $X \approx ut$, indicating that the starting shock system moves through the nozzle with nearly the same speed as the steady flow gas. But when the resident gas density is large enough for the right-hand side of (4) to approach unity, then $X \neq ut$, and the starting shock system impedes the passage of the steady flow.

Equation (4) can be very useful to the shock-tunnel experimenter who requires a rough estimate of the value of the resident gas density which is necessary to ensure rapid initiation of steady test-gas flow in the nozzle (Stalker & Mudford 1973). However, (3) is more suitable for comparison of the model with method of characteristics calculations, since it is more exact and, with prescribed distributions of the steady flow and the resident gas parameters, it is readily solved numerically. Such a comparison is shown in figure 8, for prior steady flow and no prior steady flow cases with a perfect gas. It should be noted that the perfect gas assumption is made for comparison purposes only; realization of the conditions used for the calculations

would produce strong real gas effects. The trajectories of the shock system centre of mass predicted for each case by the two methods are seen to be in good agreement, with the approximate model slightly over-predicting shock system arrival time, as expected.

It must be remembered that this analysis only yields the trajectory of the centre of mass of the starting shock system, which often may be all that is required. When a more exact estimate of details of the flow is needed, it is necessary to revert to a full numerical calculation or, for the prior steady flow case, to employ the approximate analysis which follows.

7. Approximate analysis with prior steady flow

The fact that a prior steady flow minimizes the time for which unsteady processes persist in the nozzle encourages the study of these unsteady processes in more detail.

This is done through a simplified approximate description of the mechanics of the unsteady flow, involving particularly the decoupling of the effects of area change from the unsteady wave phenomena. Remembering that a shock-tunnel experimenter will be interested in the nature and duration of the flow which precedes the steady test flow, the analysis is used to determine the velocity of the PSS, the density distribution and the spatial separation between the PSS and the SSS, as well as the contact surface between them, and to indicate the extent and strength of the unsteady expansion upstream of the SSS.

7.1. *The flow model*

As anticipated in the introduction, and confirmed in figure 2, the presence of the prior steady flow allows the PSS to propagate through the nozzle with very little change in velocity. Therefore it is assumed that the PSS velocity is constant throughout the nozzle.

Also, it is clear from figure 2 that there is only a small fractional velocity change between the PSS and the SSS, indicating that only a proportionately small change in pressure takes place between the two shocks. Thus it is assumed that the pressure is constant between them.

The model which follows from these assumptions is shown in figure 9(*a*). The PSS propagates, at constant velocity u_p, into the prior steady flow which consists of the resident gas at density ρ_r and velocity v_r. Of course, these two quantities vary with distance along the nozzle, x, and may be calculated from the equations for one-dimensional steady nozzle flow of a perfect gas. The starting shock system, which is bounded by the PSS and the SSS, also includes a contact surface, CS. This is the boundary between the post IPS gas, which has passed into the nozzle from the shock tube, and the resident gas which has been swept up by the PSS during its passage through the nozzle. The contact surface velocity is u_c, and the pressure throughout the starting shock system is constant at p_c. The starting unsteady wave is contained between the HUE and the SSS, and p_s and $u+u_s$ are the pressure and velocity immediately upstream of the SSS, while at the HUE the pressure p and the velocity u are the values obtained in the steady flow expansion of the post-IPS gas through the nozzle to the area ratio at the instantaneous station of the HUE.

7.2. *Unsteady waves with area change*

The unsteady wave between the HUE and the SSS is treated by ignoring the effect of area change in calculating the changes in flow variables across the wave.

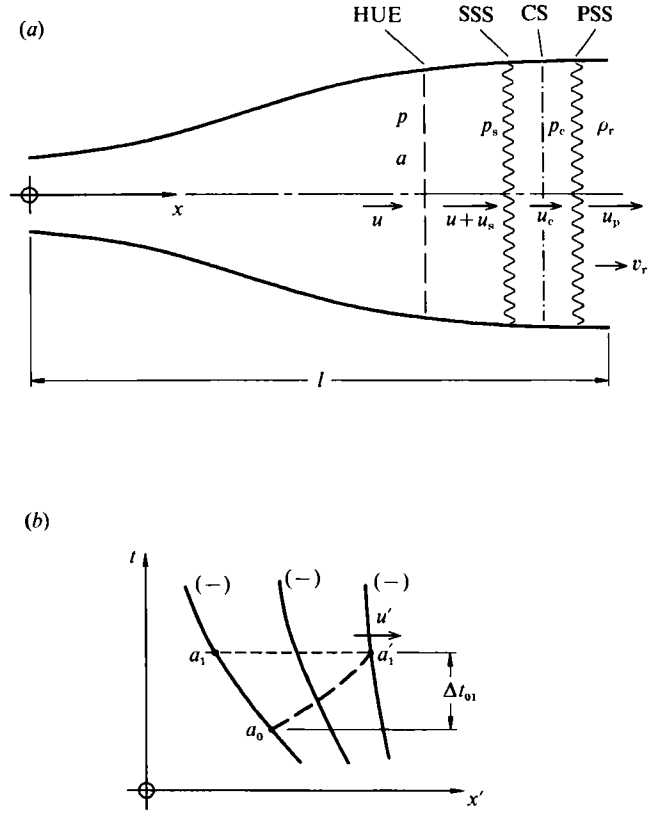

FIGURE 9. Simplified model with prior steady flow. (*a*) Flow structure; (*b*) wave diagram of unsteady expansion in constant velocity frame of reference.

The validity of this assumption may be examined by taking a frame of reference which moves along the nozzle axis with a velocity u_1, the velocity at the nozzle exit in the steady flow upstream of the HUE. A representative wave diagram of the unsteady flow in this frame of reference is shown in figure 9(*b*), with u' representing the velocity in the wave, a' and a representing the speed of sound in the wave and immediately upstream respectively, and $x' = x - u_1 t$.

Assuming homentropic flow of a perfect gas in the wave, the compatibility relations along characteristics can be written as (e.g. Rudinger 1955)

$$(\partial/\partial t)_{\pm}(2a'/(\gamma-1)\pm u') = -a'\{(u'\,\partial/\partial x' + \partial/\partial t)\ln A\}, \tag{5}$$

where γ is the ratio of specific heats, A is the nozzle cross-sectional area, and $(\partial/\partial t)_{\pm}$ represents the derivative with respect to t along (+) and (−) characteristics respectively. Both of these characteristics are represented on figure 9(*b*).

The unsteady waves considered here do not involve very large pressure ratios, and therefore the velocities generated in those waves are only of the same order as the velocity change along the nozzle in the steady expansion. Since the steady expansion is supersonic to hypersonic throughout the nozzle, it can be shown that the magnitude of u' is only one-third of u_1 or less. Further, because the nozzle contour is fixed in a laboratory frame of reference then, in the frame of reference used here

$$\partial(\ln A)/\partial t = u_1\,\mathrm{d}(\ln A)/\mathrm{d}x. \tag{6}$$

Thus the ratio of the first to the second term on the right-hand side of (5) is of the order of u'/u_1, and so the first term can be neglected. Remembering that the nozzle is axisymmetric, then

$$\mathrm{d}(\ln A)/\mathrm{d}x = 2r^{-1}\,\mathrm{d}r/\mathrm{d}x,$$

where r is the radius of the nozzle cross-section at station X, and, using (6), (5) becomes

$$(\partial/\partial t)_{\pm}(2a'/(\gamma-1)\pm u') = -2a'u_1 r^{-1}\,\mathrm{d}r/\mathrm{d}x.$$

If this is integrated along a characteristic over a time Δt_{01} which is comparable with the time taken for the unsteady wave to traverse the nozzle then, putting

$$\Delta t_{01} \sim x/u_1,$$
$$\mathrm{d}r/\mathrm{d}x \sim r/x,$$

it follows that

$$\Delta_{\pm}(2a'/(\gamma-1)\pm u') \sim -2a', \tag{7}$$

where Δ_+ and Δ_- indicate changes along $(+)$ and $(-)$ characteristics respectively.

On figure 9(*b*), following $a(+)$ and $a(-)$ characteristic respectively, for a time Δt_{01}, from an initial point 0 on the upstream $(-)$ characteristic, (7) leads to the relation

$$2(a_1-a_1')/(\gamma-1)-u' \sim -2(a_1-a_1'), \tag{8}$$

where the subscript 1 indicates values after time Δt_{01}. The right-hand side of this relation represents the effect of area change and, comparing it with the first term on the left-hand side, it is clear that it can be neglected, to a good approximation, only when

$$(\gamma-1) \ll 1. \tag{9}$$

Thus, the unsteady wave model used here can be expected to be a very approximate one indeed when $\gamma = 1.67$, as for helium test gas. But it will be more accurate for equilibrium real gas flows, where effective values of γ tend to be less than 1.2.

Neglecting the effect of area change, and eliminating the subscript 1, (8) becomes

$$a' = a-\tfrac{1}{2}u'(\gamma-1) \tag{10}$$

throughout the wave at any instant. This is the same as the relation which would apply in a simple wave in a constant area duct, originating at the local conditions given by a.

It is also worth noting that (7) can be used in combination with (10) to show that, to the same order of approximation, u' is constant along $(-)$ characteristics. This will be used below in discussing the development of the unsteady expansion.

7.3. *Contact surface and PSS velocity*

The contact surface velocity is determined by the condition that the pressure is the same, at the value p_c, on both sides of the contact surface. Now, the pressure immediately downstream of the SSS strictly is determined by allowing the gas at pressure p_s and velocity $(u+u_s)$ to pass through a shock to the velocity u_c. However, all the cases considered here involve only moderate shock pressure ratios – typically, less than 5. This allows the shock to be replaced by an unsteady simple compression wave without introducing an error greater than 8% in the pressure ratio associated with a given velocity change. Equation (10) can be applied to this compression wave, as well as to the expansion region between the HUE and the SSS, implying that homentropic relations can be applied to calculate the pressure change in all of the unsteady flow upstream of the contact surface. Therefore the pressure change from the HUE to the contact surface is given by

$$p_c/p = \{1+(\gamma-1)(u-u_c)/(2a)\}^{2\gamma/(\gamma-1)}. \tag{11}$$

IPS speed	(km s^{-1})	5.6	6.3	7.4	8.2	9.0
Shock-tube filling pressure	(kPa)	6.8	3.3	1.7	0.8	0.4
Calculated PSS speed	(km s^{-1})	6.85	7.92	8.37	8.76	9.50
Measured PSS speed	(km s^{-1})	6.5	7.6	8.0	8.3	9.8

TABLE 1. PSS velocity – comparison with experiments for air

Neglecting the static pressure in the resident gas, the pressure following the PSS can be written as

$$p_c = \rho_r(u_c - v_r)^2/(1-\epsilon_r), \tag{12}$$

where ϵ_r is the PSS inverse shock density ratio. For the resident gas, ρ_r and v_r are determined by a perfect gas calculation of the steady flow in the nozzle, with the sonic throat at the entrance to the nozzle, and the initial shock tube filling conditions taken as the reservoir conditions.

Using (11) and (12), an iterative solution can be obtained for u_c. As discussed below this involves the use of equilibrium normal shock relations for ϵ_r. The PSS velocity then can be obtained from u_c through the relation

$$u_p = (u_c - \epsilon_r v_r)/(1-\epsilon_r), \tag{13}$$

which is derived by applying continuity relations across the PSS.

For the helium test gas case of figure 2, carrying out this calculation at the nozzle exit yields a PSS velocity at the nozzle exit of 11.0 km s^{-1}, which may be compared with the value of 11.1 km s^{-1} obtained from the method of characteristics calculation.

For air, table 1 allows comparison of calculated values of the PSS velocity at the nozzle exit with values measured from interferograms similar to that in figure 7(*b*).

In general, the experimental values are approximately 5% less than the calculated ones and, making some allowance for possible increases in resident gas density owing to viscous effects in the prior steady flow, this is regarded as satisfactory agreement. At the highest IPS speed, it is thought that conditions at the helium–air interface may have led to weak compression waves which, by increasing the pressure in the post-IPS gas, caused the observed PSS speed to slightly exceed the calculated value.

7.4. *Resident gas shock layer*

As shown in figure 9, the gas initially resident in the nozzle is swept up by the PSS to form a shock layer between the contact surface and the PSS. The density immediately after passage of the PSS is $\rho_r(x)/\epsilon_r(x)$, where the x dependence of ρ_r and ϵ_r have now been made explicit. For a strong PSS in a perfect gas, $\epsilon_r(x)$ does not vary along the nozzle length. For air under the conditions of the experiments, estimates of reaction lengths indicate that densities are within 10% of equilibrium values within 3 μs after passage of the shock and, since equilibrium values of ϵ_r vary by no more than 10% along the nozzle, then the variation of the actual non-equilibrium values is expected to be of the same order.

The gas subsequently expands isentropically as it passes down the nozzle. If the small variations in $\epsilon_r(x)$ and $v_r(x)$ are neglected, then the PSS velocity becomes constant along the nozzle length, and the ratio of the post-PSS pressure at x to the post-PSS pressure at the nozzle exit is equal to the ratio of the resident gas densities at the two stations, i.e. the ratio $\rho_r(x)/\rho_r(l)$, where l is the nozzle length. Thus, for a perfect gas, the ratio of the post-PSS density at x to the density of the same element of gas as it passes the nozzle exit is

$$\{\rho_r(x)/\rho_r(l)\}^{1/\gamma},$$

and the density at the nozzle exit of an element which originated at x is given by

$$\rho_1(z) = \{\rho_r(x)/\epsilon_r(x)\}\{\rho_r(l)/\rho_r(x)\}^{1/\gamma}, \tag{14}$$

where z is the distance from the PSS as the element passes the exit. For an equilibrium real gas, the second term on the right-hand side of (14) can be obtained from a Mollier chart.

The relation between z and x is obtained by equating the mass of resident gas contained in an initial element of length $\mathrm{d}x$, at x, to that in an element of length $\mathrm{d}z$ of the post-PSS shock layer at the nozzle exit, i.e.

$$\rho_r(x)\,A(x)\,\mathrm{d}x = \rho_1(z)\,A(l)\,\mathrm{d}z.$$

It follows from this that the density reaches a value of $\rho_1(z)$ at a distance from the PSS given by

$$z = \int_l^x \{\rho_r(x)/\rho_1(z)\}\{A(x)/A(l)\}\,\mathrm{d}x, \tag{15}$$

where (14) is used for $\rho_1(z)$. Thus, the density $\rho_1(z)$ is achieved at a time t' after passage of the PSS, where

$$t' = -z/u_c. \tag{16}$$

The time history of the resident gas shock layer density distribution, for the case of helium test gas in figure 2, has been calculated by this method and, when presented as part of the figure in the top left of figure 3, is seen to agree satisfactorily with results from numerical calculations. The discrepancy between the two in the middle of the shock layer could be due to the effect of pressure gradients in the shock layer, which have been neglected here.

Calculations for air follow a similar procedure because, although the gas rapidly approaches equilibrium after the PSS, estimates indicate that negligible recombination will occur in the subsequent expansion. Therefore this part of the process can be calculated by assuming a perfect gas, with a 'frozen' value of γ determined from the equilibrium composition after the PSS.

7.5. *Secondary shock layer and the unsteady expansion*

The secondary shock layer, between the SSS and the contact surface, and the starting unsteady wave between the SSS and the HUE, have been treated as one wave for the analysis which yielded (11). In order to separate the two and to predict their main features, a more detailed approach is required.

An unsteady expansion must originate when the IPS arrives at the entrance to the nozzle, since the fact that the sonic throat for the prior steady flow occurs there ensures that the resident gas density and pressure are less than in the shock tube. The adjustment to this pressure difference occurs as the wave system passes through the steady flow field upstream of the nozzle entrance, and can be expected to take place over a distance comparable with the diameter of the entrance. This is regarded here as a sudden change which, as for a constant area flow, leads to a slight increase in the strength of the IPS as it passes into the nozzle to become the PSS, and to a weak, unsteady expansion in the post IPS flow. As noted above, the upstream head of this unsteady expansion propagates in the upstream direction at the local speed of sound with respect to the gas and, being swept downstream by the motion of the gas, becomes the HUE. This is shown, for example in figure 2.

However, it should be noted that this expansion is very weak, involving density changes which are less than 20% of the upstream density. Moreover, the dispersive

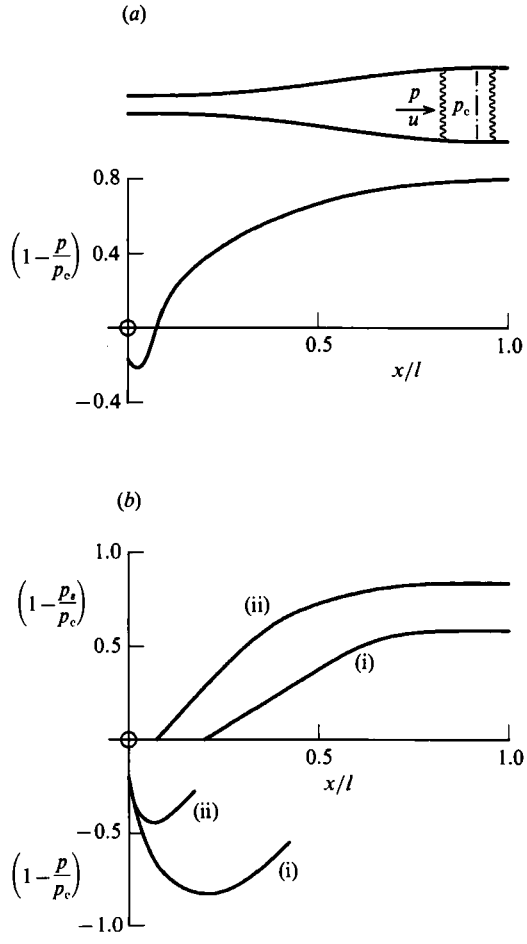

FIGURE 10. Generating the contact surface pressure. (*a*) Without unsteady expansion, helium test gas; (*b*) with unsteady expansion, air test gas. Shock-tube fill pressures (kPa): (i) 6.8; (ii) 0.4.

behaviour which is a feature of unsteady expansions ensures that the gradients of flow properties within the expansion will become very weak as it passes down the nozzle, so that it ceases to be a significant feature of the flow. This is evident in figure 3, where the expansion between the HUE and the SSS is barely noticeable on the scale of the figure.

The subsequent development of the expansion is governed by the requirement for the test gas flow in the nozzle to sustain the pressure at the contact surface, and the means of doing this depends on the relative rate of decay of p_c and p in passing through the nozzle. There are two classes of flow which result from this, and it is convenient to consider them in turn.

(i) *Monotonic decay of* p/p_c

If p decays more rapidly than p_c as the wave system passes down the nozzle, then no further expansion will be expected. Neglecting the weak initial expansion, the flow into the SSS at any nozzle station will be the steady flow in the nozzle, as shown in figure 10(*a*). The helium test gas case of figure 2 is an example of this. The pressure p_c therefore is sustained by the pressure p upstream of the SSS, together with the change of momentum of the test gas which passes through the SSS. Taking a

momentum balance across the SSS, and remembering that u_c is constant, the momentum loss, q, of the gas which passes through the SSS during its passage through the nozzle is given by the impulse of the pressure difference across the SSS, i.e.

$$q = u_c^{-1} l \int_0^1 (p_c - p) A \, \mathrm{d}(x/l),$$

and, using (12), while neglecting v_r and ϵ_r in that equation, it follows that

$$q = \rho_r A u_c l \int_0^1 (1 - p/p_c) \, \mathrm{d}(x/l), \tag{17}$$

where it has been assumed that $\rho_r A$ is constant over the nozzle length. This assumption derives from the fact that the mass flow in the nozzle is constant in the prior steady flow, and therefore $\rho_r A$ varies inversely as v_r, which is effectively constant in a hypersonic nozzle, except near the throat. There the integrand on the right-hand side of (17) tends to be small – as may be seen, for example, in the plot of $(1 - p/p_c)$ in figure 10 (*a*) – and therefore this region makes a negligible contribution to the integral.

If m_{ss} is the mass in the secondary shock layer at the nozzle exit, then q also may be written as

$$q = m_{ss}(u_1 - u_c). \tag{18}$$

This relation assumes that all of the mass which crosses the SSS previously had a velocity equal to the expanded steady flow value, u_1, an approximation which is reasonable in the hypersonic part of the nozzle. It is not a good approximation near the nozzle entrance but, as already noted in the paragraph above, the contribution to q by the flow in that region can be neglected.

Now, (11), for the pressure at the contact surface, has been obtained by assuming an isentropic compression from the steady flow to the secondary shock layer. The same assumption implies that the density is approximately constant across the secondary shock layer and indeed, this is evident in figure 3. Therefore, if y and ρ_{ss} are the thickness and density respectively of the secondary shock layer as it passes the nozzle exit then, from (17) and (18), and putting $m_{ss} = \rho_{ss} y A$, it follows that

$$y = (\rho_r/\rho_{ss})\{u_c/u_1 - u_c)\} l \int_0^1 (1 - p/p_c) \, \mathrm{d}(x/l). \tag{19}$$

Using (11) to obtain $(p_c/p)_1$, the value of the pressure ratio at the nozzle exit, the isentropic approximation then yields

$$\rho_{ss} = \rho_1 (p_c/p)_1^{1/\gamma},$$

and the thickness and the density of the secondary shock layer at the nozzle exit is determined.

This method has been used to calculate the approximate secondary shock layer density profile for the helium flow of figure 3, and is seen to give reasonable agreement with the results of the characteristics calculations.

(ii) *Initial increase of p/p_c – strengthening the unsteady expansion*

It is possible for p to decay more slowly than p_c in the upstream part of the nozzle, and then to decay more rapidly in the downstream part. For example, when the test gas following the IPS is dissociated, this can occur in the following way. The

expanding gas may remain in equilibrium in the upstream part of the nozzle, leading to a relatively slow decay in p, with an effective value of γ not much greater than unity. On the other hand, the decay of p_c is determined by the decay of ρ_r in the prior steady flow, which is a perfect gas flow with a higher value of γ. The disparity in γ for the two flows can produce a situation in which p decays more slowly than p_c.

Further down the nozzle, chemical 'freezing' may occur, producing a higher value of γ. This change in the effective value of γ then allows p to decay more rapidly than p_c. Such a situation is illustrated in figure 10(*b*), and actually occurs in the present experiments with air.

The initial increase in p/p_c produces a situation in which the pressure drops from the HUE to the contact surface, and this will strengthen any unsteady expansion which exists between the two. If p/p_c continues to increase, the expansion will become even stronger, until a maximum value of p/p_c is reached, as shown in figure 10(*b*). The strengthened unsteady expansion propagates upstream with respect to the gas, increasing the velocity and reducing the pressure of all the gas which passes through it. Subsequent to the peak value of p/p_c being achieved, the decay of p/p_c causes the SSS to form, allowing the gas which has been processed by the unsteady expansion to maintain the pressure p_c at the contact surface in the same manner as when p/p_c decays monotonically. The flow produced is as illustrated in figure 9(*a*). It is qualitatively similar to that of figure 10(*a*) with the difference that the SSS is preceded by a significant unsteady expansion.

In order to make an approximate analysis of this situation, it is assumed that the expansion wave is not overtaken by the SSS as the starting wave system passes through the nozzle. The characteristics of the unsteady expansion therefore retain their identity in the passage through the nozzle and, since it has already been argued above that the velocity change, u', generated by an expansion remains approximately constant along characteristics, it follows that the velocity change across the expansion remains constant. Thus, using the maximum value of p/p_c, and the value of a at the station where the maximum occurs, (11) can be employed to generate a velocity change across the expansion. With this velocity change, together with the values of p and a at any other station in the nozzle, the corresponding value of p_s, the pressure immediately upstream of the SSS, can be calculated. This allows the curve for $(1-p_s/p_c)$ to be constructed, as shown in figure 10(*b*) and, using this curve instead of that for $(1-p/p_c)$ and the velocity $(u+u_s)$ downstream of the unsteady expansion, rather than u, the analysis can proceed as in (ii) above to yield the thickness and the density of the secondary shock layer at the nozzle exit.

Figure 10(*b*) shows $(1-p/p_c)$ and $(1-p_s/p_c)$ as calculated for two of the conditions used in the experiments with air. When the shock tube filling pressure is 6.8 kPa, the post-IPS flow expands in equilibrium to a nozzle area ratio of 6.6, where chemical 'freezing' occurs. The curve for $(1-p/p_c)$ shows that a substantial unsteady expansion is generated during this process, and the curve for $(1-p_s/p_c)$ shows the importance of this expansion in providing the momentum to sustain the pressure p_c at the contact surface. For a shock tube filling pressure of 0.4 kPa, the expanding post-IPS flow 'freezes' close to the nozzle inlet, and a weaker expansion is generated. Nevertheless, and in contrast to the helium case of figure 10(*a*), the expansion remains strong enough to play a significant role in the development of the unsteady flow. This reveals another way in which real gas effects can influence the unsteady flow, since the expansion arises because chemical reactions after the IPS cause the Mach number at the nozzle entrance in the post-IPS flow to be higher than in the prior steady flow, and this leads to the pressure mismatch.

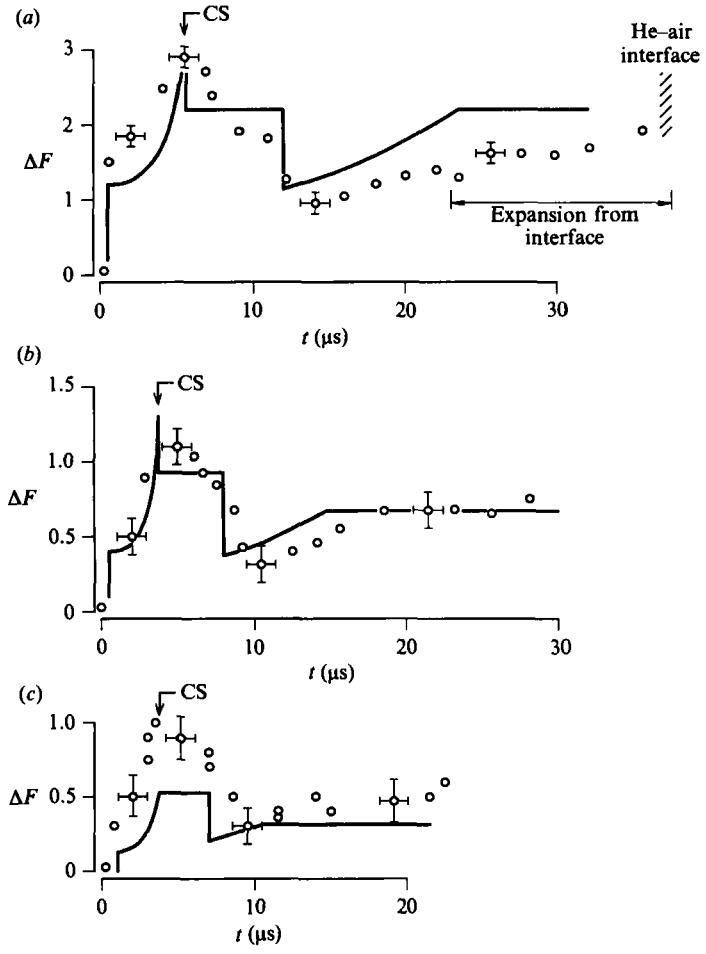

FIGURE 11. Test section flow histories in air. ○, Measured fringe shifts; —— approximate theory. Shock-tube fill pressures (kPa): (*a*) 6.8, (*b*) 1.7, (*c*) 0.4. Incident primary shock speed (km s^{-1}): (*a*) 5.6; (*b*) 7.4; (*c*) 9.0. ΔF = number of fringes shift; CS = contact surface.

Figure 11 shows measurements of fringe shift, obtained from interferograms similar to the one in figure 7 (*b*), and compares them with predictions made according to the approximate theory above. Remembering that the interferogram of figure 1 shows that the flow is only approximately one dimensional, it is seen that the PSS–SSS separation and the starting shock system density levels generally are predicted with reasonable accuracy. An exception occurs at the lowest shock-tube filling pressure, where fringe shifts clearly exceed predicted values. This could be due to a combination of viscous effects in the nozzle and the weak compression waves from the helium–air interface which have been mentioned above.

The expansion wave is generally not accurately defined in the measurements. At a shock-tube filling pressure of 6.8 kPa, calculations show that a second expansion wave may be generated at the helium–air interface as it passes through the nozzle, and this may be confusing interpretation of the measurements of the upstream part of the expansion wave of interest here. However, the predicted extent of the expansion wave is close to the measurements at the other two test conditions, as is the relative strength near the SSS at all test conditions.

The expansion wave model also can be applied to predict the effect of the weak expansion which is generated for the helium test gas case of figure 3. As shown by the dotted line on that figure, this yields a substantially stronger expansion than that obtained with the characteristics calculations, and emphasizes the very approximate nature of the expansion wave component of the model.

It is worth remarking further on the effect of possible helium–air interface generated waves. It appears that these may be influencing the steady flow region at the highest and the lowest IPS speeds. Whilst the effect has not yet been investigated systematically, it suggests that, in order to achieve the best results in non-reflected shock-tunnel operation, it may be necessary to pay attention to appropriate matching of driver gas–test gas conditions at the interface.

8. Conclusion

Studies of the unsteady flow in an expanding hypersonic nozzle indicated that the main features of the flow were the primary starting shock, the secondary starting shock, and the unsteady expansion. These were also the main features of the unsteady flow in a reflected shock tunnel nozzle, which was studied by Smith (1966). It was found that, as expected, the use of a prior steady flow in the nozzle allowed these features to pass through the nozzle with very little alteration in their speed.

Calculations, using the method of characteristics, for one-dimensional unsteady flow, successfully predicted the trajectories of the main features, as well as the variation of Pitot pressure with time for perfect gas flows. These calculations showed that the prior steady flow drastically altered the unsteady flow following the primary starting shock, by allowing that flow to accelerate from supersonic to hypersonic speeds, whereas a quiescent resident gas caused it to decelerate to subsonic speeds. These changes were reflected in the widely differing post shock density distributions in the two cases. This could be a significant factor in interpreting phenomena in explosions or pulsating exhausts, and it is certainly an important factor in establishing steady flow over a model for shock-tunnel operation.

The overall effect of resident gas density fields was accounted for by developing an approximate analytical model which allowed calculation of the trajectory of the centre of mass of the starting shock system. For all but nozzles of large area ratio with high resident gas densities, the separation between the primary starting shock and the secondary starting shock is small in relation to the distance travelled by the starting shock system and, because of this, the analytical model provides a useful means of including the effects of resident gas density fields which are different to those considered specifically here.

Approximate analysis also was used to explore details of the flow obtained when a prior steady flow existed. The model that evolved from this analysis embodied a starting shock system which was relatively thin in the streamwise direction, with constant pressure between the primary starting shock and the secondary starting shock. The expansion wave upstream of the secondary starting shock was a one-dimensional unsteady simple wave with upstream conditions given by steady flow expansion, through the nozzle, of the gas following the incident primary shock. This model yielded satisfactory predictions of the flow structure generated by characteristics calculations with helium test gas, and of that measured experimentally with air test gas.

The unsteady expansion generated in the nozzle expansion is an important feature, since it can delay the onset of steady flow following the passage of the starting shock

system. The analysis revealed the role of pressure matching in the upstream parts of the nozzle expansion in determining the strength of this expansion. With air test gas, it was seen that thermochemical effects could cause an increase in the ratio of pressure in the steady flow expansion to the pressure in the starting shock system, and thereby lead to an increase in the strength of the expansion wave upstream of the shock system. However, when this pressure ratio was close to unity, as with helium test gas, this expansion was so weak that a close approximation to steady flow was obtained immediately upon passage of the starting shock system.

This study has a significant implication for the development of experimental aerodynamics. The flight speeds associated with interplanetary exploration lead to phenomena arising from the effects of high levels of gas ionization which promise an interesting field of research, and provide an incentive to increase the flow speeds which can be achieved in shock tunnels. Studies by Hornung & Sandeman (1974), and by Logan, Stalker & McIntosh (1977) have shown that radiation from the stagnant hot gas region upstream of the hypersonic nozzle limits the performance that can be achieved by a reflected shock tunnel. The radiative power levels of the stagnant gas become so high that a large part of the internal energy of the gas is dissipated to the walls of the shock tube before a steady flow can be established in the test section and, for practical purposes, this limits the test section velocity which can be achieved. This limitation can be avoided by non-reflected shock-tunnel operation, or by expansion tube-tunnel operation, since at least half of the stagnation enthalpy of the gas remains in the form of directed kinetic energy, and cannot be radiated away. The use of prior steady flow, in the manner studied here, makes it possible to successfully operate such a shock tunnel, or expansion tube-tunnel within the short test times available with a high-velocity shock tube.

The authors would like to thank Mr R. French and Mr V. Adams for assistance during the experimental phases. The work was partly supported by the Australian Research Grants Scheme.

REFERENCES

ACKROYD, J. A. D. 1964 Studies on the running time in a shock tube and shock tunnel. PhD thesis, University of London.

DAVIES, L. 1964 Bow-shock establishment and stagnation point pressure measurements for a blunt-nosed body at supersonic speeds. *Natl Phys. Lab. Aero Rep.* 1098.

HORNUNG, H. G. & SANDEMAN, R. J. 1974 Interferometry of radiating argon flow over blunt bodies. *J. Phys.* D: *Appl. Phys.* **7**, 920.

LIEPMANN, H. W. & ROSHKO, A. 1957 *Elements of Gas Dynamics*, p. 149. J. Wiley & Sons.

LOGAN, P. F., STALKER, R. J. & MCINTOSH, M. K. 1977 A shock tube study of radiative energy loss from an argon plasma. *J. Phys.* D: *Appl. Phys.* **10**, 323.

MACROSSAN, M. N. 1990 Hypervelocity flow of dissociating nitrogen downstream of a blunt nose. *J. Fluid Mech.* **217**, 167.

MUDFORD, N. R. 1976 The production of pulsed nozzle flows in a shock tube. PhD thesis, Australian National University, Canberra.

MUDFORD, N. R. & STALKER, R. J. 1976 The production of pulsed nozzle flows in a shock tube. *AIAA paper* 76-357. (Presented at AIAA 9th Fluid and Plasma Dynamics Conference, San Diego.)

MUDFORD, N. R. & STALKER, R. J. 1980 Hypersonic nozzles for high enthalpy non-equilibrium flow. *Aero. Q.* **31**, 113.

OERTEL, H. 1970 Non-reflected shock tunnel test times. *Proc. 7th Intl Shock Tube Symp.* (ed. I. I. Glass), p. 80. University of Toronto Press.

RUDINGER, G. 1955 Wave Diagrams for Nonsteady Flow in Ducts, pp. 18–33. New York: Van Nostrand.

SMITH, C. E. 1966 The starting process in a hypersonic nozzle. *J. Fluid Mech.* **24**, 625.

STALKER, R. J. 1972 Development of a hypervelocity wind tunnel. *Aero. J. R. Aero. Soc.* **76**, 374.

STALKER, R. J. 1980 Shock tunnel measurements of ionization rates in hydrogen. *AIAA J.* **18**, 478.

STALKER, R. J. & MUDFORD, N. R. 1973 Starting process in the nozzle of a non-reflected shock tunnel. *AIAA J.* **11**, 265.